

# In-situ elasticity measurement for the unquenchable high-pressure clinopyroxene phase: Implication for the upper mantle

Jennifer Kung,<sup>1</sup> Baosheng Li,<sup>1</sup> Takeyuki Uchida,<sup>2</sup> and Yanbin Wang<sup>2</sup>

Received 1 October 2004; revised 6 December 2004; accepted 9 December 2004; published 8 January 2005.

[1] Polycrystal elasticity of the unquenchable  $\text{MgSiO}_3$  high-pressure clinoenstatite has been measured using ultrasonic interferometry in conjunction with in-situ X-ray diffraction and imaging techniques within its stability field in a large volume multi-anvil apparatus for the first time. At 6.5 GPa, we obtained  $\partial K_s/\partial P = 5.6(3)$ ,  $\partial G/\partial P = 1.5(1)$ ,  $\partial K_s/\partial T = -0.017(1)$  GPa  $\text{K}^{-1}$  and  $(\partial G/\partial T) = -0.015(1)$  GPa  $\text{K}^{-1}$ . Our results show that the elastic velocities of HP-CEN are not only higher than those of OEN but also higher than olivine at upper mantle conditions. According to these new data, the elastic velocities for the “depleted” mantle composition, with  $\sim 20$  vol% of HP-CEN, would result in  $\sim 0.8\%$  and  $\sim 1.6\%$  in difference for P and S waves, respectively, when OEN data were used in previous calculations. Newly measured results also suggest that it is possible to distinguish “undepleted” and “depleted” composition models in the upper mantle. **Citation:** Kung, J., B. Li, T. Uchida, and Y. Wang (2005), In-situ elasticity measurement for the unquenchable high-pressure clinopyroxene phase: Implication for the upper mantle, *Geophys. Res. Lett.*, 32, L01307, doi:10.1029/2004GL021661.

## 1. Introduction

[2] Ca-poor pyroxene (enstatite,  $(\text{Mg,Fe})\text{SiO}_3$ ) constitutes an average  $\sim 20$  vol% of harzburgite or the “depleted” mantle composition, which represents the average chemical composition for continental lithospheres [Jordan, 1978]. In the presence of other mantle phases, the disappearance of enstatite component through dissolution into garnet is facilitated by high Al, Ca, and Fe contents in bulk composition. In the pyrolite composition (undepleted with high Al, Ca, Fe contents relative to the “depleted” mantle composition), the enstatite phase is estimated to be exhausted above 10 GPa, corresponding to a depth of  $\sim 300$  km, as indicated by the experiments of Irifune [1987]. In situations where Al, Ca, Fe contents are low (i.e., in harzburgite or “depleted” mantle compositions), the enstatite dissolution is minimal. This makes enstatite as an unique mantle phase in differentiating the two compositional models at deeper depths of the upper mantle, where the thickness of continent roots is a long time debate [e.g., Anderson, 1979; Jordan, 1981; Lerner-Lam and Jordan, 1987; LeFevre and Helmberger, 1989]. The enstatite component often exhibits an orthorhombic symmetry (space

group Pbca, orthoenstatite, OEN) in mantle specimens. High pressure experiments [Pacalo and Gasparik, 1990; Angel *et al.*, 1992] revealed a high-pressure monoclinic polymorph (high-pressure clinoenstatite, or HP-CEN hereafter; space group C2/c) in enstatite above  $\sim 8$  GPa, corresponding to the mantle depth below 250 km. As shown by Angel *et al.* [1992], the crystal structure of the  $\text{MgSiO}_3$  HP-CEN phase cannot be retained in the recovered sample at low pressures (below  $\sim 6$  GPa). Hence, the elasticity data for this phase must be obtained in-situ within its stability field. This non-quenchable nature has severely limited the experimental studies on the HP-CEN phase. Due to the absence of experimental data on HP-CEN, elasticity data of the OEN phase were often used in the calculation of the elastic properties for the proposed thermal and compositional models for comparison with seismic observations at upper mantle conditions [e.g., Duffy and Anderson, 1989; Vacher *et al.*, 1998; Cammarano *et al.*, 2003]. This has contributed to uncertainties in the estimated elastic properties of the upper mantle.

[3] The implementation of X-radiography in ultrasonic measurement combined with in-situ X-ray diffraction studies has made it possible to monitor the change of the sample length along with the simultaneous measurement of travel time and density of the sample [Kung *et al.*, 2002, 2004; Li *et al.*, 2004]. Using these state-of-the-art experimental techniques, we have successfully measured the elastic wave velocities of unquenchable HP-CEN within its stability field and were able to determine its thermoelastic properties in a self-consistent manner. Here we present the elasticity of  $\text{MgSiO}_3$  HP-CEN at high pressure and temperature, and its implication.

## 2. Experimental Techniques and Procedures

[4] Ultrasonic measurements at high pressures and temperatures in conjunction with synchrotron X-radiation were performed on polycrystalline specimens of  $\text{MgSiO}_3$ -high pressure clinoenstatite in a 1000-ton multianvil press [Uchida *et al.*, 2002] installed at the 13-ID-D beamline of GSECARS, the Advanced Photon Source, Argonne National Laboratory. Experimental details were reported by Kung *et al.* [2004] and therefore are described briefly here. During the experiments, the HP-CEN specimens were first synthesized at  $\sim 13$  GPa and  $\sim 1273$  K for two hours using well-sintered  $\text{MgSiO}_3$  orthoenstatite specimens as the starting material, which were hot-pressed prior to the ultrasonic experiments. After the specimen has fully transformed to the HP-CEN phase, as confirmed by X-ray diffraction at these P-T conditions, experimental data were collected along a series of heating/cooling paths in decompression to provide a reasonable coverage in P-T space, within the

<sup>1</sup>Mineral Physics Institute, State University of New York at Stony Brook, Stony Brook, New York, USA.

<sup>2</sup>GeoSoilEnviroCARS, Center for Advanced Radiation Sources, University of Chicago, Chicago, Illinois, USA.

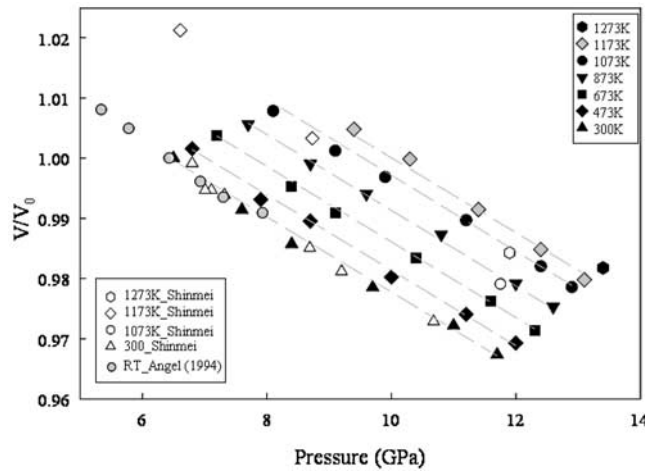


**Figure 1.** Comparison of the unit-cell volumes (shown as  $V/V_0$ , reference state is 6.5 GPa, room temperature) for  $\text{MgSiO}_3$  HP-CEN at various pressure and temperature from this study (solid symbols) and previous studies, *Angel and Hugh-Jones* [1994] (circles in grey) and *Shinmei et al.* [1999] (open symbols). The cell volume at 6.5 GPa, room temperature for *Angel and Hugh-Jones* [1994] is  $385.0 \text{ \AA}^3$  and for *Shinmei et al.* [1999] is  $384.2 \text{ \AA}^3$ , refitted from their P-V-T data.

stability field of HP-CEN [Kung et al., 2004, Figure 1]. Experiments were terminated at  $\sim 6$  GPa, below which pressure the HP-CEN phase is known to transform to the low-pressure clinoenstatite phase (space group  $P2_1/c$ ) at low-temperature regime [Angel et al., 1992; Ross and Reynard, 1999], or to OEN at high-temperature regime (T. Gasparik, personal communication, 2002).

[5] Two runs (T354 and T409) with two different specimens were carried out. At each P-T condition, both P and S wave travel times, sample length, and cell parameters for both the specimen and NaCl were collected. Cell volumes of NaCl were used to determine the cell pressures, based on the equation of state proposed by Decker [1971]. Due to the weak intensity of X-ray data for the HP-CEN phase collected in run T354 (complicated by the cell assembly used; for details see Kung et al. [2004]), no unit cell volumes were obtained from this run. Consequently, the equation of state of the HP-CEN phase was determined using the data from run T409 only.

### 3. Results and Discussion

[6] For convenience, we chose 6.5 GPa and 298 K as the reference state for data presentation of the HP-CEN phase in this study. The entire P- $V_{\text{volume}}$ -T dataset (up to 1273 K, from 6 to 14 GPa) was fit to a third-order Birch-Murnaghan equation of state with a specific expression for the high temperature volume at the pressure of the reference state:  $V_0(T) = V_0(T_0) \exp[\alpha_0(T - T_0) + 1/2\alpha_1(T^2 - T_0^2)]$ , using program EoS-fit v5.2 [Angel, 2001]. We constrained the isothermal bulk modulus and its pressure derivative using in-situ measured acoustic data at the reference state ( $K_S = 156.7(8) \text{ GPa}$ ,  $K'_S = 5.5(3)$  [Kung et al., 2004, Table 3]) to extract the thermal expansivity  $\alpha(T)$  and temperature derivative of the isothermal bulk modulus at these conditions. The

adiabatic bulk modulus has been converted to isothermal value,  $K_T = 155(1) \text{ GPa}$  (the conversion factor  $K_S/K_T = (1 + \alpha\gamma T) \approx 1.01$  was employed). No correction was made between  $\partial K_T/\partial P$  and  $\partial K_S/\partial P$  in this study because the difference is significantly less than the uncertainty in the measured pressure derivatives. The refined unit cell volume at 6.5 GPa room temperature,  $385.0(3) \text{ \AA}^3$ , is in good agreement with our observed value,  $385.6(1) \text{ \AA}^3$ , as well as the value at 6.4 GPa reported by *Angel and Hugh-Jones* [1994],  $385.0(1) \text{ \AA}^3$ . We obtained a result of  $\alpha(T) = 1.73(80) \times 10^{-5} + 1.64(1.17) \times 10^{-8}T$  and  $(\partial K_T/\partial T) = -0.025(10) \text{ GPa K}^{-1}$ . The value of  $(\partial K_T/\partial T)$  derived from P-V-T data is in good agreement with the value of  $-0.023(2) \text{ GPa/K}$  converted from acoustic measurement ( $\partial K_S/\partial T = -0.017$ , see next section), when  $\gamma \approx 1.16$  (estimated using  $\gamma = -1/6 + 0.024(\partial K_S/\partial P) + 0.799(\partial G/\partial P)$ , [Anderson, 1995, equation 1.73]) and  $\alpha(T)$  from above is used. Compared with previous studies, the volume measurements (Figure 1, shown as  $V/V_{(6.5\text{GPa}, 298\text{K})}$ ) from this study agree very well with those of *Angel and Hugh-Jones* [1994] and *Shinmei et al.* [1999] at room temperature, implying a similar pressure derivative of isothermal bulk modulus ( $\partial K_T/\partial P$ ) among three studies. In comparison with high-temperature data of *Shinmei et al.* [1999] (Figure 1), the relative volumes ( $V/V_{(6.5\text{GPa}, 298\text{K})}$ ) measured from this study are systematically higher, amounting to  $\sim 0.7\%$  at 1273K. Constrained by the same bulk modulus and pressure derivative used in this study, the dataset of *Shinmei et al.* [1999] suggested a more negative value for  $(\partial K_T/\partial T)$  ( $-0.042(5) \text{ GPa/K}$ ) than our current value ( $-0.025(10) \text{ GPa/K}$ ). The discrepancy may be due to the fact that the high-temperature properties are not well-constrained by their dataset, since there are limited high-temperature data points collected by *Shinmei et al.* [1999] (11 out of 24). In contrast, the equation of state derived from this study not only had denser data coverage in P-T space, it was also constrained by simultaneous in-situ elasticity measurements; reliable equation of state result for the  $\text{MgSiO}_3$  HP-CEN phase was therefore assured.

[7] The compressional (P) and shear (S) wave velocities, determined from the measured travel times and specimen lengths, are plotted as a function of pressure at high temperature (Figure 2). Both P and S wave velocities from runs T354 and T409 exhibit linear increase with pressure along each isotherm. The elastic velocities determined from these two runs are comparable; the maximum difference in velocities between these two runs is  $\sim 0.5\%$  at temperature of 1073 K at peak pressure. The bulk ( $K_S$ ) and shear ( $G$ ) moduli at high pressure and temperature are subsequently calculated from the measured P and S wave velocities and densities ( $K_S = \rho(V_P^2 - 4/3V_S^2)$  and  $G = \rho V_S^2$ ). To obtain pressure and temperature derivatives, the bulk and shear moduli data are treated as linear functions of pressure and temperature. The fitting results are  $K_S = 156(1) \text{ GPa}$ ,  $G = 99(1) \text{ GPa}$ ,  $(\partial K_S/\partial P) = 5.6(3)$ ,  $(\partial G/\partial P) = 1.5(1)$ ,  $(\partial K_S/\partial T) = -0.017(1) \text{ GPa K}^{-1}$  and  $(\partial G/\partial T) = -0.015(1) \text{ GPa K}^{-1}$ . The resultant elastic moduli and their pressure derivatives are in good agreement with those obtained at room temperature ( $K_S = 156.7(8) \text{ GPa}$ ,  $G = 98.5(4) \text{ GPa}$ ,  $(\partial K_S/\partial P) = 5.5(3)$ ,  $(\partial G/\partial P) = 1.5(1)$  at 6.5 GPa [see Kung et al., 2004, Table 3]).

[8] In the uppermost mantle (above 400 km),  $\text{MgSiO}_3$  polymorphs and olivine are the most abundant phases in the

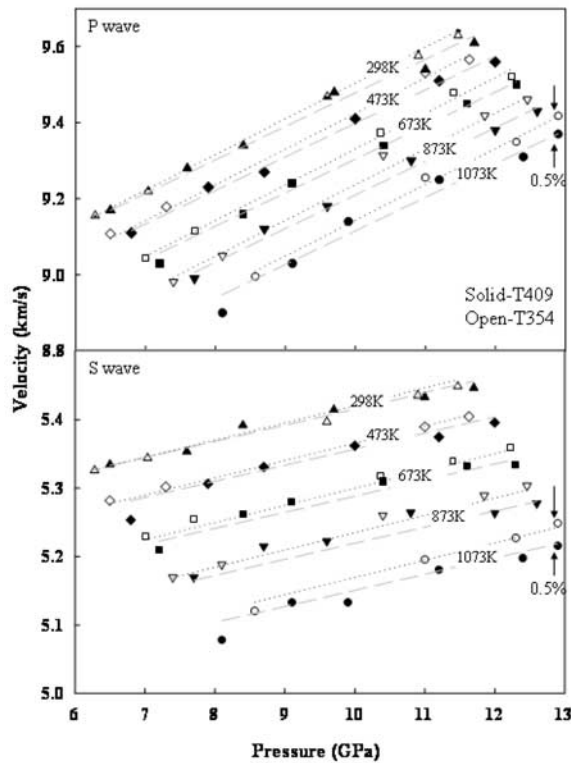


**Figure 2.** P and S wave velocities in  $\text{MgSiO}_3$  HP-CEN phase as function of pressure and temperature from run T354 and T409.

mantle composition models; their thermoelastic properties at the corresponding pressure and temperature conditions provide valuable information on interpreting the observed seismic profiles in terms of composition and temperature. Before the elasticity of HP-CEN was measured, the pyroxenes (except Na-pyroxene) used to be considered as “slow” materials in the mantle when compared to olivine [e.g., *Duffy and Anderson, 1989*]. With our newly measured elasticity for HP-CEN, we are now able to re-evaluate the physical state of  $\text{MgSiO}_3$  polymorphs at upper mantle conditions.

[9] The elastic velocities for olivine,  $\text{MgSiO}_3$ -OEN and -HP-CEN were calculated along an adiabatic temperature of 1673 K at high pressures using a similar approach of *Duffy and Anderson* [1989]. The thermoelastic properties of these three phases used in our calculation are summarized in

Table 1. Some selected elastic constants ( $C_{ij}$ ) of the OEN phase were measured up to high temperature, room pressure by *Jackson et al.* [2004], however, they are insufficient to calculate the bulk elasticity properties for the aggregates. In this study, the temperature derivatives of the elastic moduli were assumed to be similar to those of HP-CEN. For the purpose of comparison, the velocity calculations for olivine and OEN were carried out up to 14 GPa; although the OEN phase would transform into HP-CEN above  $\sim 8$  GPa at high temperature. The elastic velocities for HP-CEN were calculated from 6.5 to 14 GPa. Owing to the starting state of the HP-CEN phase, at 6.5 GPa and room temperature, its elastic velocities were calculated along a 1773 K adiabat at 6.5 GPa to match the conditions for which the olivine and OEN phases were calculated. The resultant P and S wave velocities for olivine,  $\text{MgSiO}_3$  OEN and HP-CEN are plotted in Figure 3. As clearly seen in Figure 3, both P and S wave velocities for OEN increase as function of pressure and gradually converge towards olivine at high pressures (i.e., within the HP-CEN stability field, shown as the dotted line in Figure 3) but are still lower than those of olivine. In comparison, S wave velocities of HP-CEN are systematically  $\sim 5.2\%$  higher than olivine at all pressures. For P wave, the velocity differences between HP-CEN and olivine are small at 6.5 GPa and gradually increase to  $\sim 2\%$  at 14 GPa. The velocity differences at high temperature between OEN and HP-CEN were estimated to be  $\sim 4\%$  for P wave and  $\sim 7.8\%$  for S wave at pressures between 6.5 to 14 GPa.

[10] Chemically, the HP-CEN phase is expected to be present in a “depleted” mantle composition rather than an “undepleted” (or the pyrolite mantle) composition at deeper part of the upper mantle. The “depleted” composition is characterized by an assembly of olivine and enstatite components of more than 85 vol%. Due to the small velocity difference in P wave between HP-CEN and olivine, HP-CEN appears to be seismically “invisible” while coexisting with olivine. On the other hand, the presence of HP-CEN would make a noticeable contribution to the S wave velocity in the “depleted” composition. *Cammarano et al.* [2003] calculated the seismic velocity of the upper mantle using OEN data instead of HP-CEN and found that the differences between the “undepleted” and “depleted” mantle composition models are less than 0.5% throughout the upper-mantle (above 400 km) along the same adiabatic geotherm. According to the results in Figure 3, at the depths where HP-CEN is a stable phase in the mantle, the calculated elastic velocities for the “depleted” mantle

**Table 1.** Elastic Properties of  $\text{MgSiO}_3$  Polymorphs and  $\text{Mg}_2\text{SiO}_4$  Olivine

		$K_S$	G	$\partial K_S/\partial P$	$\partial G/\partial P$	$\partial K_S/\partial T$ GPa K <sup>-1</sup>	$\partial G/\partial T$ GPa K <sup>-1</sup>	$\partial K_T/\partial T$ GPa K <sup>-1</sup>	Remark
$\text{MgSiO}_3$	HP-CEN	156(1)	99(1)	5.6(3)	1.5(1)	-0.017(1)	-0.015(1)	-0.025(10)	@6.5 GPa, RT
	OEN <sup>a</sup>	108(1)	77(1)	7.2(7)	1.7(1)				
	OEN					-0.017 <sup>b</sup>	-0.015 <sup>b</sup>	-0.025 <sup>c</sup>	
$\text{Mg}_2\text{SiO}_4$	Olivine <sup>d</sup>	125	81	4.5(2)	1.4(1)	-0.014(1)	-0.017(1)	-0.022(2)	
	Olivine <sup>e</sup>	129	82			-0.016	-0.014		
	Olivine <sup>f</sup>	129	82	4.2	1.4				

<sup>a</sup>Kung et al. [2004].

<sup>b</sup>Temperature derivatives of the elastic moduli for OEN are assumed to be the same as those of HP-CEN.

<sup>c</sup> $\partial K_T/\partial T$  for OEN is refined from the P-V-T dataset summarized by *Angel* [2001].

<sup>d</sup>Li et al. [2004].

<sup>e</sup>Isaak et al. [1989].

<sup>f</sup>Duffy et al. [1995].



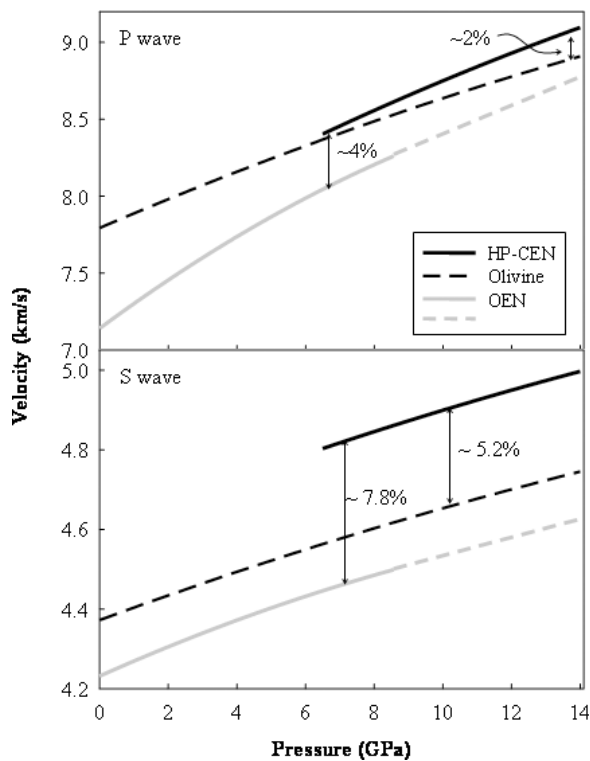


**Figure 3.** Comparison of the P and S wave velocity for  $\text{MgSiO}_3$ -OEN (grey lines) and -HP-CEN (black solid line), and  $\text{Mg}_2\text{SiO}_4$ -olivine (black dashed line, calculated from data in Table 1) under mantle pressure and temperature. The velocities of OEN calculated within the stability of HP-CEN were marked as grey dashed line.

compositional model, with an average of  $\sim 20$  vol% of HP-CEN, could be underestimated by about 0.8% and 1.6% for P and S waves, respectively, when the elasticity of HP-CEN was replaced with OEN data. As a result, the magnitude of these velocity differences between the “depleted” and “undepleted” could be different from those inferred by Cammarano *et al.* [2003], especially in S wave. This observation suggests that it is possible to distinguish the two compositional models in terms of elastic properties. Further study including a complete modeling of composition and temperature effects on the seismic profiles in the upper mantle using updated elasticity data will shed light on the unresolved issue of the thickness of continental lithosphere.

[11] **Acknowledgments.** We thank for the support of beamline 13-ID, GSECARS. This study is supported by the National Science Foundation under the Grants EAR0229704 to R.C.L. and EAR0003340 to B.L.. Use of the Advanced Photon Source was supported by the U.S. Department of Energy, Office of Science, Office of Basic Energy Sciences, under Contract No. W-31-109-ENG-38. GSECARS is supported by the National Science Foundation - Earth Sciences, Department of Energy - Geosciences, W. M. Keck Foundation, and the U.S. Department of Agriculture. MPI publication No. 352.

## References

Anderson, D. L. (1979), Deep-structure of continents, *J. Geophys. Res.*, **84**, 7555–7560.

- Anderson, O. L. (1995), The free energy and the Grüneisen parameter, in *Equations of State of Solids for Geophysics and Ceramic Science*, edited by O. L. Anderson, p. 28, Oxford Univ. Press, New York.
- Angel, R. J. (2001), Equations of state, in *High-Pressure, High-Temperature Crystal Chemistry*, *Rev. in Mineral. Geochem.*, vol. 41, edited by R. M. Hazen and R. T. Downs, pp. 35–60, Mineral. Soc. of Am., Washington, D. C.
- Angel, R. J., and D. A. Hughes-Jones (1994), Equations of state and thermodynamic properties of enstatite pyroxenes, *J. Geophys. Res.*, **99**, 19,777–19,783.
- Angel, R. J., A. Chopelas, and N. L. Ross (1992), Stability of high-density clinoenstatite at upper-mantle pressures, *Nature*, **358**, 322–324.
- Cammarano, F., S. Goes, P. Vacher, and D. Giardini (2003), Inferring upper-mantle temperatures from seismic velocities, *Phys. Earth Planet. Inter.*, **138**, 197–222.
- Decker, D. L. (1971), High-pressure equation of state for NaCl, KCl, and CsCl, *J. Appl. Phys.*, **42**(8), 3239–3244.
- Duffy, T. S., and D. L. Anderson (1989), Seismic velocities in mantle minerals and the mineralogy of the upper mantle, *J. Geophys. Res.*, **94**, 1895–1912.
- Duffy, T. S., C. S. Zha, R. T. Downs, H. K. Mao, and R. J. Hemley (1995), Elasticity of forsterite to 16 GPa and the composition of the upper-mantle, *Nature*, **378**, 170–173.
- Irfune, T. (1987), An experimental investigation of the pyroxene garnet transformation in a pyrolite composition and its bearing on the constitution of the mantle, *Phys. Earth Planet. Inter.*, **45**, 324–336.
- Isaak, D. G., O. L. Anderson, T. Goto, and I. Suzuki (1989), Elasticity of single-crystal forsterite measured to 1700 K, *J. Geophys. Res.*, **94**, 5895–5906.
- Jackson, J. M., S. V. Sinogeikin, M. A. Carpenter, and J. D. Bass (2004), Novel phase transition in orthoenstatite, *Am. Mineral.*, **89**, 239–244.
- Jordan, T. H. (1978), Composition and development of continental tectosphere, *Nature*, **274**, 544–548.
- Jordan, T. H. (1981), Continents as a chemical-boundary layer, *Philos. Trans. R. Soc. London, Ser. A*, **301**, 359–373.
- Kung, J., B. Li, D. J. Weidner, J. Z. Zhang, and R. C. Liebermann (2002), Elasticity of  $(\text{Mg}_{0.83}\text{Fe}_{0.17})\text{O}$  ferropericlasite at high pressure: Ultrasonic measurements in conjunction with X-radiation techniques, *Earth Planet. Sci. Lett.*, **203**, 557–566.
- Kung, J., B. Li, T. Uchida, Y. Wang, D. Neuville, and R. C. Liebermann (2004), In situ measurements of sound velocities and densities across the orthopyroxene→high-pressure clinopyroxene transition in  $\text{MgSiO}_3$  at high pressure, *Phys. Earth Planet. Inter.*, **147**, 27–44.
- LeFevre, L. V., and D. V. Helmberger (1989), Upper mantle P velocity structure of the Canadian shield, *J. Geophys. Res.*, **94**, 17,749–17,765.
- Lerner-Lam, A. L., and T. H. Jordan (1987), How thick are the continents?, *J. Geophys. Res.*, **92**, 14,007–14,026.
- Li, B., J. Kung, and R. C. Liebermann (2004), Modern techniques in measuring elasticity of Earth materials at high pressure and high temperature using ultrasonic interferometry in conjunction with synchrotron X-radiation in multi-anvil apparatus, *Phys. Earth Planet. Inter.*, **143–144**, 559–574.
- Pacalo, R. E. G., and T. Gasparik (1990), Reversals of the orthoenstatite-clinoenstatite transition at high-pressures and high-temperatures, *J. Geophys. Res.*, **95**, 15,853–15,858.
- Ross, N. L., and B. Reynard (1999), The effect of iron on the P2(1)/c to C2/c transition in  $(\text{Mg,Fe})\text{SiO}_3$  clinopyroxenes, *Eur. J. Mineral.*, **11**, 585–589.
- Shinmei, T., N. Tomioka, K. Fujino, K. Kuroda, and T. Irfune (1999), In situ X-ray diffraction study of enstatite up to 12 GPa and 1473 K and equations of state, *Am. Mineral.*, **84**, 1588–1594.
- Uchida, T., et al. (2002), A large-volume press facility at the advanced photon source: Diffraction and imaging studies on materials relevant to the cores of planetary bodies, *J. Phys. Condens. Matter*, **14**, 11,517–11,523.
- Vacher, P., A. Mocquet, and C. Sotin (1998), Computation of seismic profiles from mineral physics: The importance of the non-olivine components for explaining the 660 km depth discontinuity, *Phys. Earth Planet. Inter.*, **106**, 275–298.

J. Kung and B. Li, Mineral Physics Institute, State University of New York at Stony Brook, Stony Brook, NY 11794-2100, USA. (jennifer.kung@sunysb.edu)

T. Uchida and Y. Wang, GSECARS, Center for Advanced Radiation Sources, University of Chicago, Chicago, IL 60639, USA.